Thin Solid Films 582 (2015) 56–59

Contents lists available at ScienceDirect

Thin Solid Films

journal homepage: www.elsevier.com/locate/tsf

Effects of NaF evaporation during low temperature Cu(In,Ga)Se_2 growth

B. Bissig *, P. Reinhard, F. Pianezzi, H. Hagendorfer, S. Nishiwaki, S. Buecheler, A.N. Tiwari

Laboratory for Thin Films and Photovoltaics, Empa, Swiss Federal Laboratories for Materials Science and Technology, Ueberlandstrasse 129, Duebendorf 8600, Switzerland

ARTICLE INFO

Available online 15 November 2014

Keywords:
Copper Indium gallium selenide
Post-deposition treatment
Admittance spectroscopy
Alkali
Sodium
SIMS
ICP-MS

ABSTRACT

Co-evaporation of NaF during the 3rd stage of the low temperature Cu(In,Ga)Se_2 multi-stage process is compared to post-deposition treatment (PDT) with NaF in view of their influence on the electronic and structural properties. In case of NaF co-evaporation, quantum efficiency losses in the near infrared region and thus lower short circuit current density cause a reduced efficiency compared to solar cells prepared with NaF PDT. The formation of a deep defect with activation energy of ~250 meV is measured by capacitance spectroscopy and can explain the deteriorated performance in such devices. In addition, NaF co-evaporation during the 3rd stage causes reduced grain size in the top part of Cu(In,Ga)Se_2 and altered In, Ga, and Cu distribution.

1. Introduction

Alkali elements and the way they are introduced in Cu(In,Ga)Se_2 (CIGS) layers play a recurring role in the efficiency improvement of solar cells. The necessity to add dilute amounts of alkali elements to the CIGS layer is known for more than two decades [1]. Traditionally, they have been incorporated by diffusion at high temperature from soda lime glass (SLG) substrates during CIGS growth. In case of alkali free substrates such as polyimide (PI) co-evaporation or precursor strategies were first investigated [2–6]. Despite its well-known beneficial effects on device properties, Na was found to decrease CIGS grain size [2,5], reduce the minority carrier lifetime [7], and affect the Cu and Ga distribution when added during absorber growth [2,5]. It was also realized by our group that the beneficial effects of Na on electronic properties can be effectively isolated from its effect on CIGS growth properties by a post-deposition treatment (PDT) with NaF [4,8].

CIGS for highly efficient solar cells is often grown by a 3-stage process. In the 1st stage In and Ga are co-evaporated together with Se. During the 2nd stage, Cu and Se are added until a Cu rich composition is achieved. Finally, in the 3rd stage, In, Ga, and Se are supplied again until an overall Cu poor absorber is reached. Our group reported that addition of NaF during the 3rd CIGS deposition stage yields similarly efficient solar cells as compared to NaF PDT, whereas addition of NaF during the 1st and 2nd stage [5] typically leads to lower PV performance.

In a previous study, we showed that KF co-evaporation during the 3rd stage induces the formation of a deep defect, which is absent when KF is added by a PDT, and discussed its effects on electronic properties [9]. To investigate to what extend this also happens when NaF is co-evaporated, and as an attempt to further increase the carrier concentration while avoiding the unfavorable effects of early Na incorporation, we focus on NaF co-evaporation during the 3rd stage after a Cu-poor composition is reached. Therefore, in the following we compare NaF co-evaporation to a PDT approach with respect to effects on electronic and compositional device properties while keeping the total amount of supplied NaF fixed in all cases.

2. Experimental details

CIGS solar cells were deposited on Mo coated PI substrates. The ~2.5 μm thick absorbers were grown by co-evaporation at a maximum substrate temperature of 450 °C in a high vacuum chamber equipped with an additional NaF effusion cell. A modified 3-stage process (multi-stage process) similar to the one described by Chirilă et al. [8] was used. Final [Cu]/([Ga] + [In]) (CGI) values determined by XRF range between 0.78 and 0.82 and the [Ga]/([Ga] + [In]) (GGI) ratios are between 0.36 and 0.38. NaF was evaporated either during the whole 3rd stage (5′–20′), or only for a reduced time (5′–11′) but with a higher rate, see Fig. 1, at a substrate temperature of 450 °C. During the PDT, NaF was evaporated for 20 min at a substrate temperature of ~350 °C, as described by Chirilă et al. [8]. The total flux of NaF is similar in all cases. Solar cells were finished with a CdS buffer layer, an i-ZnO/ZnO:Al front contact, a metal grid, and an anti-reflective coating following our standard recipe [10] .

The photovoltaic (PV) parameters of the solar cells were extracted from current density–voltage (*J*–*V*) characteristics under simulated standard test conditions (1000 W/m^2, 25 °C, AM1.5G) measured with a Keithley 2400 source meter with four terminal sensing. External quantum efficiency (EQE) curves were obtained using a lock-in amplifier from Stanford Research Systems and chopped light from a halogen lamp. An Agilent E4980A LCR meter was used for capacitance–frequency

* Corresponding author. Tel.: +41 58 765 43 05; fax: +41 58 765 1112.
E-mail address: benjamin.bissig@empa.ch (B. Bissig).

http://dx.doi.org/10.1016/j.tsf.2014.11.026
0040-6090/

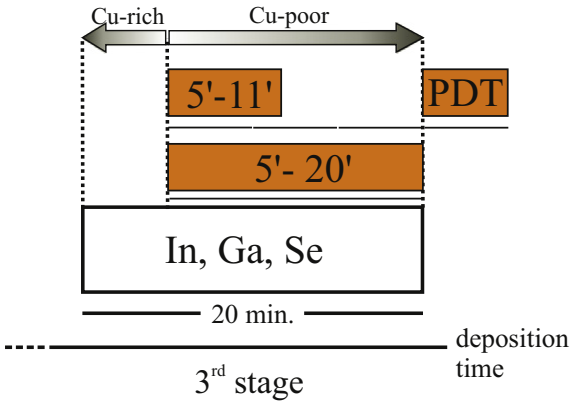

Fig. 1. Schematics showing the 3rd stage of CIGS deposition with two NaF co-evaporation windows indicated as boxes. Additionally, the post-deposition treatment (PDT) is shown where NaF is evaporated after CIGS deposition at reduced substrate temperature of ~350 °C.

(*C–f*) and capacitance–voltage (*C–V*) measurements. *C–f*, *C–V*, and illumination-dependent *J–V* measurements were performed in the range from 120 K to 340 K in a cryostat cooled with liquid nitrogen. All capacitance measurements were performed in relaxed state, i.e., devices were stored for at least 30 min in dark before cooling. Reverse saturation current density j_0, its activation energy E_{j0}, and the diode ideality factor A were extracted from illumination and temperature-dependent J_{SC}–V_{OC} measurements, as described by Nadenau et al. [11]. Elemental depth profiles were performed with time-of-flight secondary ion mass spectrometry (ToF-SIMS5, ION-TOF), and for the quantification of Na in CIGS, inductively coupled plasma mass spectrometry (ICP-MS) was used. Experimental details are given elsewhere [8]. Scanning electron microscopy (SEM) was performed in a Hitachi S-4800 SEM at 5 keV acceleration voltage and a working distance of 5.2 mm.

3. Results

3.1. Effects on composition and morphology

Fig. 2 compares Na, In, Ga, and Cu elemental depth profiles in the top 350 nm of the CIGS layer through completed devices where Na was introduced after (PDT) or during (5′–11′ and 5′–20′) the 3rd deposition stage after the layer becomes Cu-poor. The time window where NaF was co-evaporated is reflected in the Na profile close to CdS/CIGS interface with a Na count rate up to ~2 orders of magnitude higher relative to the PDT treated sample. A spiked Na signal is observed in the 5′–11′ case, whereas the count rate appears more plateau like in the 5′–20′ case. The absolute Na concentrations with respect to the CIGS layer as measured by ICP-MS are given in Table 1. The SEM micrograph in Fig. 3 shows the cross section of the NaF PDT and 5′–20′ sample. A significant decrease in grain size is observed in the top region of the absorber when NaF is co-evaporated instead of a PDT. Atom probe tomography of CIGS layers revealed that Na resides mainly at grain boundaries [12,13], which can explain the higher absolute Na content and the increased SIMS Na count rate with respect to CIGS in our samples. Similar effects on grain size and SIMS profiles were previously reported in case of NaF [2–6] and KF [9] co-evaporation.

Table 1
Comparison of PV parameters, diode ideality factor A, reverse saturation current density j_0, and its activation energy E_{j0} of the different devices. Further shown are the apparent carrier density N_{CV} as determined by *C–V* profiling and defect energies E_{def} as extracted from *C–f* spectra as well as the Na concentrations with respect to the CIGS layer determined by ICP-MS.

Sample	PDT	5′–11′	5′–20′
J_{sc} (mA/cm^2)	33.4	32.6	31.5
V_{OC} (mV)	694	684	690
FF (%)	78.2	75.3	75.2
Eff. (%)	18.1	16.8	16.4
A	1.4	1.3	1.3
j_0 (mA/cm^2)	1.4×10^{-7}	1.5×10^{-7}	8.5×10^{-8}
E_{j0} (eV)	1.19	1.22	1.19
N_{CV} (cm^{-3})	2×10^{15}	1×10^{16}	1×10^{16}
E_{def} (meV)	–	250	250
Na (at%)	0.05	0.38	0.65

3.2. Effects on electronic properties

Table 1 compiles the PV parameters of the solar cells with the three different absorbers. Na introduction during the 3rd deposition stage decreases the cell efficiency with respect to PDT. This loss is mainly caused by a decrease in short circuit current (J_{SC}) and fill factor (FF). The diode ideality factor, j_0 and E_{j0} do not indicate a clear difference in recombination mechanism for the three cases. All E_{j0} are close to Eg ~1.15 eV, and the ideality factors are about ~1.4, indicating recombination in the space charge region. Furthermore, a decreasing J_{SC} was observed at low temperatures (not shown).

EQE curves are shown in Fig. 4. An overall reduction in EQE is observed when NaF was present during CIGS deposition. Further, the 5′–20′ sample suffers from increased losses in the near infrared (NIR) region. Typically, such NIR losses arise due to short minority carrier diffusion length or due to incomplete absorption. Given the comparable GGI values and similar absorber thickness, we will discuss our results in terms of a defect related model in the following.

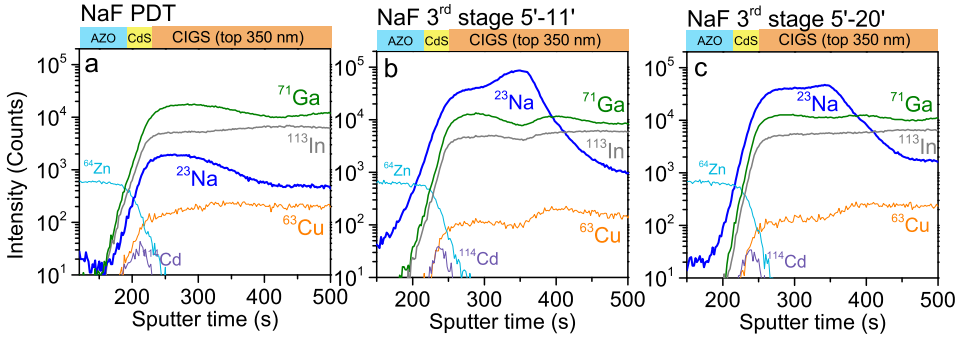

Fig. 2. SIMS depth profiles showing the top ~350 nm of the absorber for the samples with different Na introduction strategies. The time intervals of Na introduction are closely reflected in the SIMS profiles. Cu, In, and Ga signals are locally reduced where Na yield increases.